Influence of the Stiffness and Saturated Conditions of Sand on the Numerical Simulation of Free Fall Penetrometers

Luis E. Zambrano-Cruzatty, S.M.ASCE[1]; Alba Yerro, Ph.D.[2]; and Nina Stark, Ph.D., M.ASCE[3]

[1]Dept. of Civil and Environmental Engineering, Virginia Polytechnic Institute and State Univ., Blacksburg, VA. E-mail: luisez@vt.edu
[2]Dept. of Civil and Environmental Engineering, Virginia Polytechnic Institute and State Univ., Blacksburg, VA. E-mail: ayerro@vt.edu
[3]Dept. of Civil and Environmental Engineering, Virginia Polytechnic Institute and State Univ., Blacksburg, VA. E-mail: ninas@vt.edu

Downloaded from ascelibrary.org by VPI & SU on 06/08/20. Copyright ASCE. For personal use only; all rights reserved.

ABSTRACT

Impact penetration into soils is one of the most challenging phenomena to model using numerical techniques due to the very rapid large-deformations and water-soil-structure interaction problems involved in the process. In this work, portable free fall penetration testing (FFP) in dry and saturated sands is modeled using the material point method (MPM). MPM is a powerful tool for large-deformation applications in history-dependent materials. A parametric analysis is performed to understand the influence of the soil stiffness and the water excess pore pressures produced during the impact. The effect of the sand stiffness is studied by modifying its Young's modulus, and the effect of the water is considered by comparing a fully dry model with a fully coupled hydro-mechanical model. The results indicate that the stiffness of the sand strongly controls the appearance of a general bearing capacity failure, which produces deceleration responses with more than one peak, dissimilar to physical tests. In the case of fully saturated sand, the penetration depth is lower than for dry sand with the same properties and the kinematical response of the FFP is consistent with experiments. The results are promising and encourage further development of the simulations.

INTRODUCTION

The Material Point Method (MPM) is a powerful tool to tackle problems involving large-deformation in geotechnical engineering (Yerro et al. 2013) because it handles those deformations without the difficulties associated with mesh tangling. MPM can also incorporate the behavior of history-dependent materials, which is the case of soils (Al-Kafaji 2013; Yerro 2015). Since it was first published by Sulsky et al. (1995), several improvements have been proposed, such as contact algorithms (Bardenhagen et al. 2000; Bardenhagen et al. 2001), multi-phase formulations (Al-Kafaji 2013; Yerro 2015), among others. These features make MPM suitable for modeling problems in geotechnics that would be complicated with other methods. Examples of large-deformation problems with MPM include the study of landslides run-out (Yerro 2015; Yerro et al. 2018), progressive failure in brittle soils (Zabala and Alonso 2011; Yerro et al. 2016), pile installation (Phuong et al. 2014), CPT testing (Ceccato et al. 2016a; Ceccato et al. 2016b), and impact penetration problems (Zambrano-Cruzatty and Yerro 2019; Zambrano-Cruzatty et al. 2019). Among these problems, impact penetration is one of the most challenging phenomena to model because it consists of large deformations, dynamic soil-structure interaction, coupling between pore pressures and soil response, transient strain-rates, and complex soil constitutive behavior (Nazem et al. 2012; Wang et al. 2015). Free Fall Penetrometer (FFP) testing is one of such problems.

© ASCE

Downloaded from ascelibrary.org by VPI & SU on 06/08/20. Copyright ASCE. For personal use only; all rights reserved.

In FFP testing, a probe of fluid dynamic shape or features falls "freely" through water or air and impacts into the soil with impact velocities reaching up to ~7 m/s (Albatal et al. 2019). After the impact, the FFP penetrates the ground until resistance forces applied by the sediments overcome the momentum. During the penetration, the FFP measures its ac-/deceleration and pore pressure response of the soil. In Figure 1, an example of experimental data measured (penetration depth vs. velocity and penetration depth vs. deceleration) from FFP deployments in dry and saturated sand is presented using the portable free fall penetrometer *BlueDrop* (Albatal2018).

One of the primary purposes of using a FFP is to characterize the geomechanical properties associated with seafloor sediments. Most recently, more studies have focused on sandy seabeds where the friction angle (ϕ') represents a most common property used to approach problems such as bearing capacity, scour predictions, among others (Stark et al. 2009; Stark et al. 2012; White et al. 2018). Hence, it is highly desirable to obtain these properties from FFP testing measurements. To do so, it is necessary to filter out the effects of the High Strain-Rate (HSR) from the records. These effects include the viscous component of the soi strength which is not straightforward to analyze. Hence, there is the necessity to perform numerical studies of FFP testing. Previous simulations of FFP deployment have been performed (Aubeny and Shi 2006; Carter et al. 2010; Nazem et al. 2012; Moavenian et al. 2016) using different Finite Element Method (FEM) techniques, which often require rigorous and computationally expensive re-meshing algorithms to overcome the mesh tangling. Moreover, the majority of the authors have studied the problem in clay, and only Zambrano-Cruzatty et al. (2019) presented a model in sand. Therefore, there is a clear lack of numerical simulations of FFP testing in such soils.

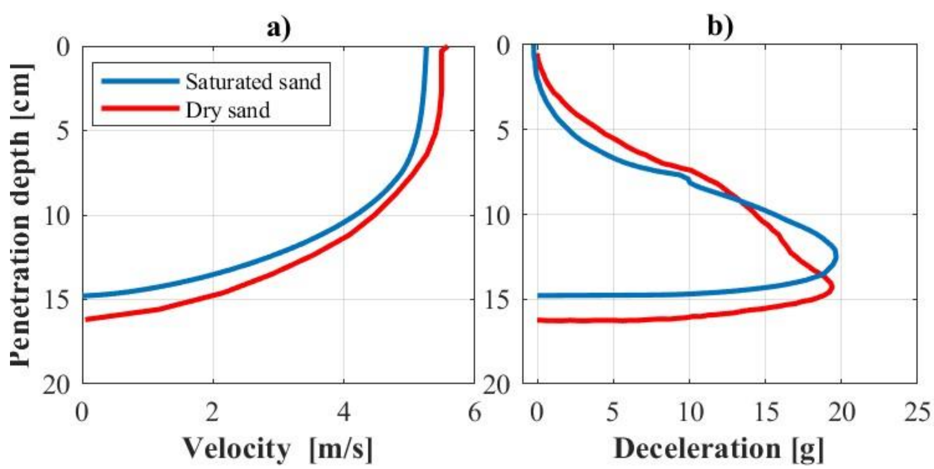

Figure 1. Experimental FFP test performed using the portable FFP *BlueDrop* in saturated and dry loose sand (Albatal 2018). a) Velocity profile, and b) deceleration profile.

This study consists of investigating the influence of the sand's stiffness and the water effect in the porous media using the MPM numerical framework by performing a parametric analysis of the Young's modulus (*E'*) and a hydro-mechanical coupled formulation. The paper is organized as follows. First, a brief description of the MPM is presented. Then, the constitutive model and soil properties are discussed. Afterward, the details and features of the numerical simulation are introduced, followed by the discussion of the results obtained. Finally, the concluding remarks and future work are included.

© ASCE

Downloaded from ascelibrary.org by VPI & SU on 06/08/20. Copyright ASCE. For personal use only; all rights reserved.

THE MATERIAL POINT METHOD

MPM is an extension of the Fluid Implicit Particle (FLIP) in cell method for solid mechanics problems (Sulsky et al. 1995). In MPM, the material is discretized by a set of integration points (i.e., material points) where the mass, kinematic variables (e.g., acceleration, velocity, and displacement), stress, strain, and state variables are stored. Initially, the properties of the material points are mapped to a background mesh, where the governing equations (i.e., momentum balances) are solved. The numerical scheme required to solve the governing equations is called Lagrangian phase, and is similar to the standard FEM scheme. After the Lagrangian phase, the updated solution is transferred back to the material points, where the mass balance and constitutive equations are posed. Finally, the position of the material points is updated, and the information of the mesh is discarded. This stage is the so-called Convective phase, and because of the mesh remains typically unchanged, it resembles a Eulerian description of the movement. By using this approach, MPM can handle large-deformation problems overcoming the difficulties associated with both Lagrangian and Eulerian frameworks. Mesh tangling is avoided and the state variables related to history-dependent materials can be rigorously tracked (Yerro 2015).

Additionally, MPM can handle multi-phase formulations. Al-Kafaji (2013), Martinelli (2016), and Yerro (2015) presented coupled formulations for two and three-phase analysis, which allow the modeling of a variety of problems in which a strict representation of drainage conditions is required. The formulation of a two-phase analysis consists of solving three different momentum balance equations; these are the momentum balance of the solid phase, the liquid phase, and the mixture of solid and liquid. However, only two of these equations are required to be solved because they are not fully independent (i.e., one can be expressed in terms of another).

The study proposed here has been performed with the internal version of the Anura 3D MPM software (http://anura3d.com). Anura 3D can handle two-phase analysis in two distinct modes: 1) Using a single set of material points in which each material point carries information of the two phases, or 2) using two sets of material points, in which each set represents each phase as a single continuum. A comparison of both formulations is presented in (Ceccato et al. 2018). In this study, the first option is adopted.

NUMERICAL SIMULATION

In this section, the main details of the numerical simulation are discussed. These features are the geometrical configurations, mesh, and boundary conditions; and the constitutive modeling of the sand.

Geometry, mesh, and boundary conditions: The geometry of the problem is based on a set of experiments performed by Albatal (2018). In those experiments the *BlueDrop* FFP (http://bluecdesigns.com) is dropped into a sand container (Figure 2a). The numerical model consists of a 20° cylindrical slice with overall dimensions of 1.1 m height and 0.4 m of diameter (Figure 2b).

Several mesh configurations have been analyzed to optimize the model performance. A fine zone (1 cm) has been considered where the rupture mechanism occurs (Figure 2a), whereas it is coarse in other zones. The mesh elements are four nodded tetrahedrons. The "moving mesh" concept is adopted to ensure that the FFP shape and contact surface is kept well defined during the simulation (Al-Kafaji 2013). The moving mesh consists of subdividing the domain into a "moving area" which moves accordingly to the FFP movement, and a "compressing area" that

© ASCE

contracts at the same rate. The sand and FFP material assignation are shown in Figure 2b. Ten material points per element are considered for the sand in the zone of mesh refinement, and four points per element in the coarser mesh. One point per element is considered for the FFP. With this configuration, a total of 177,112 material points are taken into account for calculations. Normally fixed boundary conditions are assigned to the symmetry axis, the top and bottom surface, and the lateral planes of the cylindrical slice. For the curved face, only the vertical movement is allowed. All the faces are specified as impervious boundaries when saturated conditions are assumed. The initial stresses are calculated using a K_o procedure.

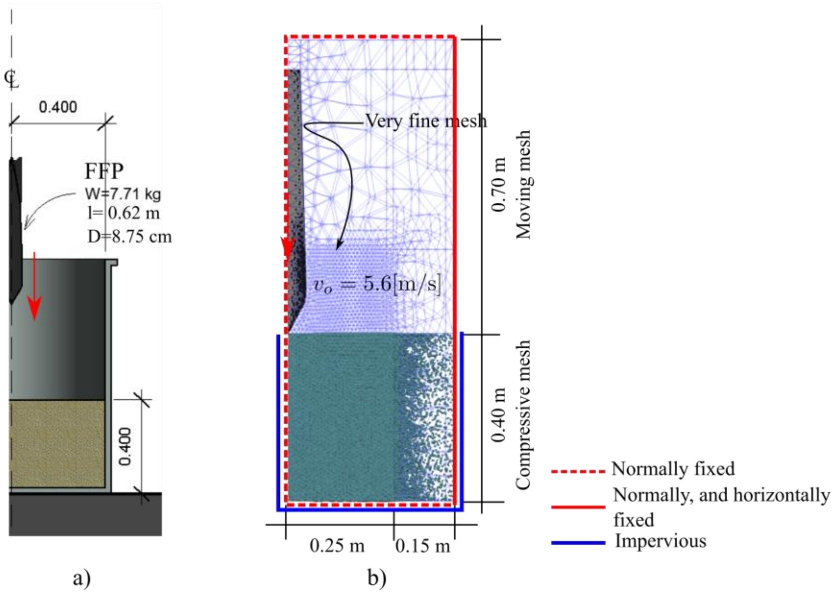

Figure 2. Geometrical details of the numerical modeling. a) Experimental setup, and b) numerical domain showing the mesh, material point density, and boundary conditions.

Materials: To study the effect of the stiffness of the sand, it is desirable to account for a constitutive model that offers some simplicity in the analysis. Because of that, in this study, the Mohr-Coulomb (MC) constitutive equation is employed. The sand is simulated with a dry unit weight of $\gamma_d = 14.6$ kN/m^3, porosity $n = 0.44$, and permeability $k = 0.01$m/s. A friction angle of $\phi' = 40°$ and zero cohesion are assigned to it. The Poisson's ratio is set to ν' = 0.33, and the coefficient of lateral earth pressure at rest is set to $K_o = 0.39$. The Young's modulus is varied between 1,000 kPa to 20,000 kPa to study the sand's stiffness effect.

The FFP is simulated as a rigid body with a weight of 7.71 kg, and it is put at immediate contact with the soil with an initial velocity of 5.6 m/s. The apex angle is 60°, and a slightly smoothed curvature is added to circumvent numerical instabilities. The soil-FFP interaction is simulated using the contact algorithm proposed by Bardenhagen et al. (2001) with a contact friction of $\delta = 20°$ (Zambrano-Cruzatty and Yerro 2019).

RESULTS

In this section, the numerical results are presented and analyzed. The objectives are: a) to understand the effect of the soil stiffness on the simulation by doing a parametric analysis changing the Young's modulus of the sand; b) to explain the role of drainage in the simulation of FFP testing by comparing the 1-phase fully dry simulation with a fully coupled hydro-

Downloaded from ascelibrary.org by VPI & SU on 06/08/20. Copyright ASCE. For personal use only; all rights reserved.

Downloaded from ascelibrary.org by VPI & SU on 06/08/20. Copyright ASCE. For personal use only; all rights reserved.

mechanical model in saturated sand.

Stiffness influence: The stiffness of the sand during a penetration process is controlled by the strain-rates at which the penetration takes place. It is well known that an increasing strain-rate will increase the Young's modulus (Omidvar et al. 2012), therefore it is important to study its influence in an FFP simulation. To achieve that purpose, nine simulations have been prepared with Young's modulus ranging from *E'* = 1,000 kPa to *E'* = 20,000 kPa. The friction angle, cohesion, and Poisson's ratio are identical for all the models and are set according to section 3. The selected range is based on reported experiments (Albatal 2018), low confining pressures, and by considering an increase of 115% due to strain rates (Yamamuro et al. 2011). All models in this parametric analysis are performed assuming dry sand, and the air in the porous is not accounted (i.e., excess of pore air pressure is neglected).

The numerical results show two different behaviors of the FFP penetration as the stiffness increases (Figure 3 and 4). The transition is found to be between *E'* = 2,500 kPa and *E'* = 5,000 kPa. Note that for comparison purposes, the results with softer sands (*E'* ≤ 2,500 kPa, Figure 3) are presented separately from those with stiffer sands (*E'* > 2,500 kPa, Figure 4). The penetration depth time-histories (Figure 3a and 4a) show that despite the stiffness, the final penetration is similar, in this case around 19 cm. Consistently, the FFP bouncing is more enlarged in the softer materials (Figure 3a) than in the stiffer ones (Figure 4a). This effect can also be appreciated in the velocity profiles (Figures 3b and 4b) where the velocity becomes negative indicating that FFP bounces back (dashed line designates $v = 0$). Another difference is that softer sands tend to overestimate the velocities, while an insignificant difference in velocities is observed for the stiffer ones.

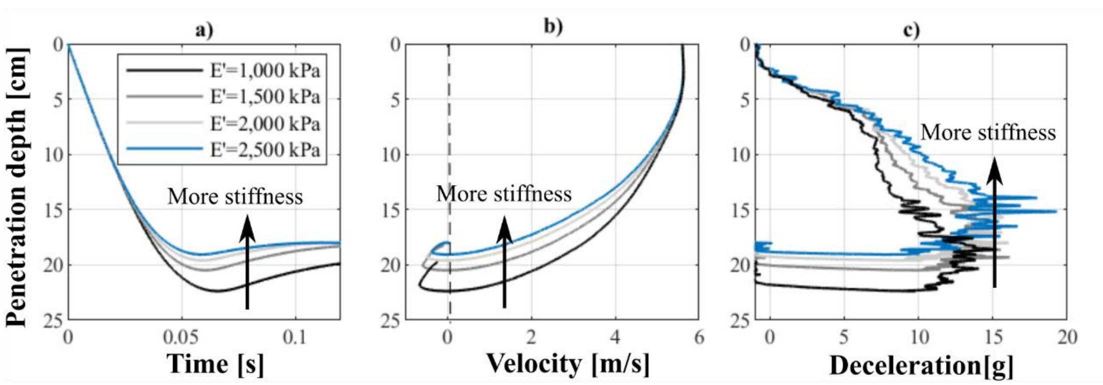

Figure 3. MPM simulations for Young's modulus from 1,000 kPa to 2,500 kPa. a) Penetration depth time-history, b) velocity profile, and c) deceleration profile.

The deceleration profiles are presented in Figures 3c and 4c and are congruent with the velocity plots. A "secondary peak" deceleration (enclosed by the red dashed lines in Figure 4c) is recorded between t=0.04 s and t=0.06 s when stiffer materials are considered. This secondary peak is more accentuated when the Young's modulus is larger. Contrarily, the deceleration profile of softer materials (Figure 3c) shows a unique peak, which is more similar to the behavior observed in the laboratory experiments by Albatal (2018). Besides the different behaviors, it is evident that i) the Young's modulus has a minor influence in the maximum deceleration, which is about 15 g for all the cases (Figures 3 and 4), and ii) as the stiffness increases, the maximum deceleration occurs earlier and shallower.

The occurrence of the secondary peak deceleration seems to be clearly associated with the development of localized shear bands conforming a general bearing capacity failure. To illustrate

© ASCE

Downloaded from ascelibrary.org by VPI & SU on 06/08/20. Copyright ASCE. For personal use only; all rights reserved.

this, the deviatoric strain contour plots are shown for two representative cases: E' = 1,000 kPa (Figure 5a), and E' = 20,000 kPa (Figure 5b). The plots are presented at two different instants, before and after the secondary peak occurs (0.04s ≤ t ≤ 0.06s). Consistent behavior is observed for all the simulations. In other words, when the bearing capacity failure mechanism is developed, a secondary peak deceleration is formed (Figure 5b), while when the bearing failure mechanism is not formed, a secondary deceleration peak is not observed, and instead, a more localized failure is developed around the FFP (Figure 5a). An explanation for this phenomenon is that as the stiffness increases, the material constitutive model (MC) approaches a rigid perfectly-plastic behavior, and the general bearing capacity failure mechanism is developed consistently with the closed form solutions such as the Terzaghi's bearing capacity theory. Accordingly, the passive wedge (Figure 5b) becomes kinematically unstable, reducing the horizontal confinement of the FFP and allowing it to decelerate at a minor rate. The last is opposed by the soil below the wedge, and a secondary peak deceleration is recorded.

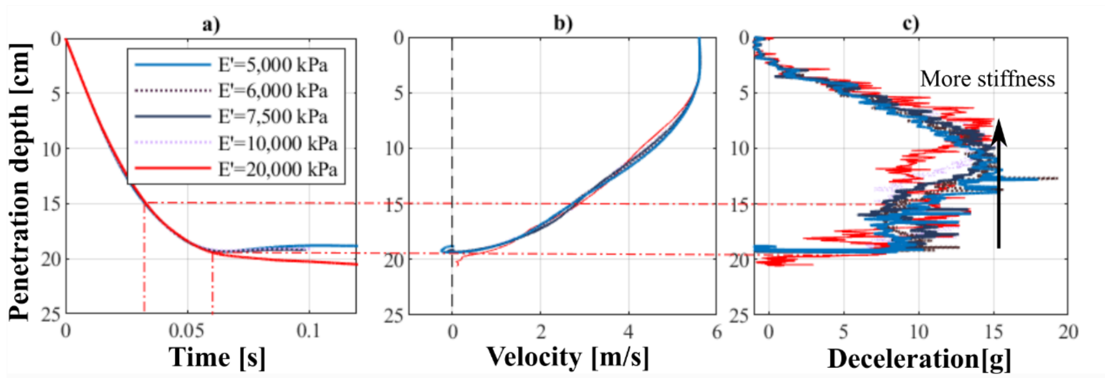

Figure 4. MPM simulations for Young's modulus from 5,000 kPa to 20,000 kPa. a) Penetration depth time-history, b) velocity profile, and c) deceleration profile.

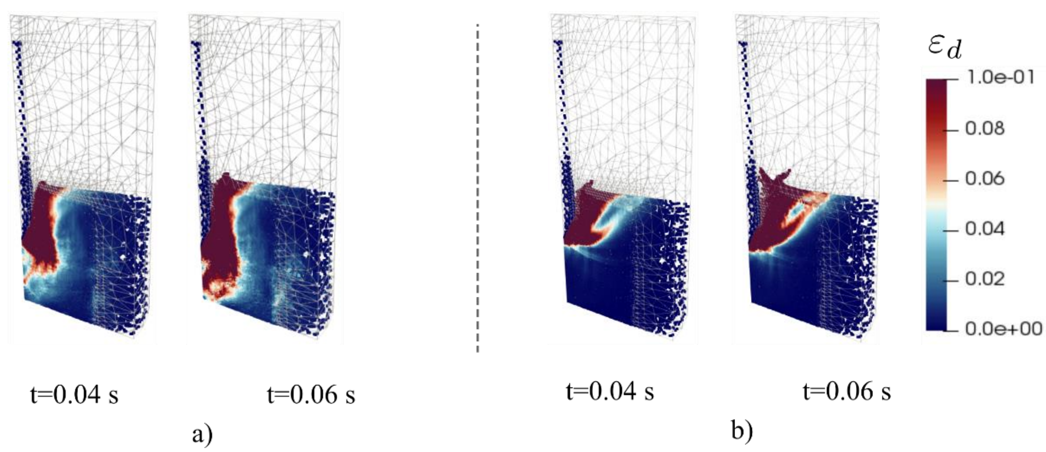

Figure 5. Deviatoric strain contour plots for two different stiffness modulus. a) *E'*=1,000 kPa, and b) *E'*=20,000 kPa.

Coupled Hydro-mechanical analysis: Although FFP testing can be performed in dry sands (e.g., in coastal dunes), it is mostly used for underwater applications. Hence, the effect of water in the soil and the drainage conditions of sands during the deployment of FFP are important. Sands can have a drainage transition between undrained, partially drained, and fully drained behavior at HSR (Albatal 2018; White et al. 2018), which imposes a constriction on the

© ASCE

Downloaded from ascelibrary.org by VPI & SU on 06/08/20. Copyright ASCE. For personal use only; all rights reserved.

numerical formulation required to asses changeable drainage behavior. In this section, the FFP deployment into saturated sand is analyzed taking into account a fully coupled hydro-mechanical formulation. In this way, the excess pore pressure can be naturally generated as a result of the FFP impact and can only dissipate through the ground surface. An initial hydrostatic pore water pressure distribution is assumed. A Young's modulus of E' = 5,000 kPa has been considered for reference, while the rest of the material parameters are identical to those presented in section 3.

Contrary to the behavior observed in the model with dry sand for the same Young's modulus, the fully coupled analysis does not present a general bearing capacity failure mechanism (Figure 6a). Consistently, the velocity profile smoothly decreases (Figure 6b), and a secondary peak deceleration is not observed (Figure 6c). The maximum deceleration occurs at the end of the penetration, and subsequently, it sharply decreases down to zero. Moreover, the penetration depth for the saturated sand (15 cm) is shallower than for the dry sand (19 cm). One possible explanation for the different behavior is that the fully coupled simulation is damped by the Darcy's velocity component in the governing equations, which incorporates a viscous effect in the solution. This could explain the shallower penetration depth compared to the drained analysis. Besides, when the sand tends to expand as a result of the deformation process, negative pore water pressures are developed, and because the penetration is rapid, they do not have time to dissipate, resulting in an apparent increase of the material strength. In practice, all sands exhibit dilation tendency during penetration processes (Yamamuro et al. 2011; Omidvar et al. 2012), hence this mechanism can generate even higher negative excess pore pressure in the shear band, reducing even further, its penetration and preventing the full development of the general bearing capacity failure (similar to a CU triaxial test in dense sands). Although a more advanced constitutive model is required to catch all components of volume change properly, it is reasonable that the transient drainage in saturated sands, impede the shear band localization and the subsequent formation of the secondary deceleration peak.

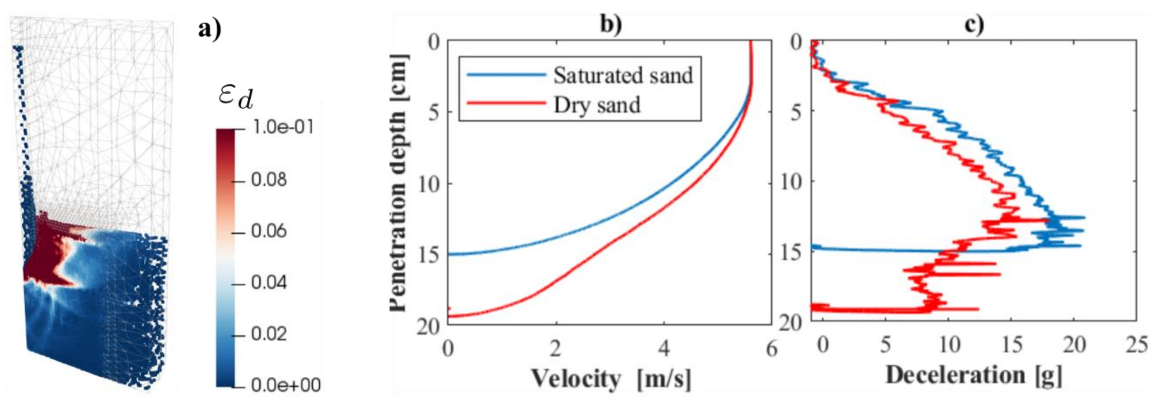

Figure 6. MPM results with saturated conditions: a) deviatoric strain, b) velocity profile, c) deceleration profile. Results with dry conditions are included for reference.

CONCLUSIONS

This work studies a) the effect of the sand's stiffness and b) the influence of dry/saturated conditions during FFP deployment. It is found that the soil stiffness controls the behavior of dry sand in fully drained conditions. For stiffer materials, the formation of a general bearing capacity failure mechanism is developed, while for softer materials, a more local failure is observed around the FFP. The transition Young's modulus that separates the two behaviors has been detected between E' = 2,500 kPa and E' = 5,000 kPa. The failure mechanism influences the

© ASCE

deceleration recordings, and the development of a general failure mechanism can be directly related to the appearance of a secondary peak in the deceleration profile. The material stiffness has a minor influence in a) the final penetration depth and in b) the magnitude of the maximum deceleration, which are found to be around 19 cm and 15 g respectively for the simulations performed in this work. Other effects of the Young's modulus are that for softer materials, as the stiffness decreases, the bouncing of the FFP increases and a tendency to overestimate the velocities is observed in the velocity profiles. On the other hand, for stiffer materials, there is a negligible difference between the velocities during the penetration. Generally, as the stiffness increases the maximum peak deceleration occurs earlier and at shallower depths.

For the simulation performed in saturated sand, although it is performed with "stiff" sand (E' = 5,000 kPa), a general bearing capacity failure is not developed and, consistently, the deceleration profile does not present a secondary peak. The FFP penetration depth is shallower than for the dry case (15 cm and 19 cm respectively). Despite the simplicity of the constitutive model (Mohr-Coulomb) the general behavior obtained with MPM is consistent with experimental observations (Albatal 2018), hence the results are promising and encouraging.

Future work will be focused on performing a more exhaustive validation of the model in dry and saturated conditions by comparing with field and laboratory tests. Moreover, the selection of more advanced constitutive equations including high strain rate effects will be taken into consideration.

ACKNOWLEDGEMENTS

The authors want to thank Virginia Tech for the funding provided, Dr. Ali Albatal, and Dennis Kiptoo for providing the experimental data.

REFERENCES

Al-Kafaji, I. K. J. (2013). "Formulation of a Dynamic Material Point Method (MPM) for Geomechanical Problems." Ph.D. thesis, University of Stuttgart, Stuttgart.

Albatal, A. (2018). "Advancement of using portable free fall penetrometers for geotechnical site characterization of energetic sandy nearshore areas." Ph.D. thesis, Virginia Polytechnic Institute and State University, Blacksburg.

Albatal, A., Stark, N., & Castellanos, B. (2019). "Estimating in situ relative density and friction angle of nearshore sand from portable free fall penetrometer tests." *Canadian Geotechnical Journal*, (ja)

Aubeny, C. P. and Shi, H. (2006). "Interpretation of Impact Penetration Measurements in Soft Clays." *Journal of Geotechnical and Geoenvironmental Engineering*, 132(6), 770–777.

Bardenhagen, S.G., Brackbill, J.U., andSulsky, D. (2000). "The material-point method for granular materials." *Computer Methods in Applied Mechanics and Engineering*, 187(3-4), 529–541.

Bardenhagen, S. G., Guilkey, J. E., Roessig, K. M., Brackbill, J. U., Witzel, W. M., and Foster, J. C. (2001). "An improved contact algorithm for the material point method and application to stress propagation in granular material." *CMES - Computer Modeling in Engineering and Sciences*, 2(4), 509–522.

Carter, J. P., Nazem, M., Airey, D. W., and Chow, S. H. (2010). "Dynamic Analysis of Free-Falling Penetrometers in Soil Deposits." *GeoFlorida 2010: Advances in Analysis, Modeling & Design*, 53–68.

Ceccato, F., A., Y., and Martinelli, M. (2018). "Modelling soil-water interaction with the

Downloaded from ascelibrary.org by VPI & SU on 06/08/20. Copyright ASCE. For personal use only; all rights reserved.

© ASCE

Material Point Method. Evaluation of single-point and double-point formulations." *Proceedings of the European Conference on Numerical Methods in Geotechnical Engineering*, Porto, Portugal.
Ceccato, F., Beuth, L., and Simonini, P.(2016a). "Analysis of Piezocone Penetration under Different Drainage Conditions with the Two-Phase Material Point Method." *Journal of Geotechnical and Geoenvironmental Engineering*, 142(12), 04016066.
Ceccato, F., Beuth, L., Vermeer, P.A., and Simonini, P.(2016b). "Two-phase Material Point Method applied to the study of cone penetration." *Computers and Geotechnics*, 80, 440–452.
Martinelli, M. (2016). "Soil-water interaction with material point method. double-point formulation." *Report no* mpm-dredge piap-ga-2012-324522., Deltares.
Moavenian, M. H., Nazem, M., Carter, J. P., and Randolph, M. F. (2016). "Numerical analysis of penetrometers free-falling into soil with shear strength increasing linearly with depth." *Computers and Geotechnics*, 72, 57–66.
Nazem, M., Carter, J., Airey, D., and Chow, S. (2012). "Dynamic analysis of a smooth penetrometer free-falling into uniform clay." *Géotechnique*, 62(10), 893–905.
Omidvar, M., Iskander, M., and Bless, S. (2012). "Stress-strain behavior of sand at high strain rates." *International Journal of Impact Engineering*, 49, 192–213.
Phuong, N., van Tol, A., Elkadi, A., and Rohe, A. (2014). "Modelling of pile installation using the material point method (MPM)." *Numerical methods in Geotechnical engineering*, 271–276.
Stark, N., Wilkens, R., Ernstsen, V. B., Lambers-Huesmann, M., Stegmann, S., & Kopf, A. (2012). "Geotechnical properties of sandy seafloors and the consequences for dynamic penetrometer interpretations: quartz sand versus carbonate sand." *Geotechnical and Geological Engineering*, 30(1), 1-14.
Stark, N., Hanff, H., and Kopf, A. (2009). "Nimrod: A tool for rapid geotechnical characterization of surface sediments." *Sea Technology*, 50(4), 10–14.
Sulsky, D., Zhou, S., and Schreyer, H. L. (1995). "Application of a particle-in-cell method to solid mechanics." *Computer Physics Communications*, 87, 236–252.
Wang, D., Bienen, B., Nazem, M., Tian, Y., Zheng, J., Pucker, T., and Randolph, M. F. (2015). "Large deformation finite element analyses in geotechnical engineering." *Computers and Geotechnics*, 65, 104–114.
White, D. J., O'Loughlin, C. D., Stark, N., and Chow, S. H. (2018). "Interpretation of free fall penetrometer tests in sands: An approach to determining the equivalent static resistance." *Cone Penetration Testing 2018*, 695–701.
Yamamuro, J. A., Abrantes, A. E., and Lade, P. V. (2011). "Effect of Strain Rate on the Stress-Strain Behavior of Sand." *Journal of Geotechnical & Geoenvironmental Engineering*, 137(12), 1169–1178.
Yerro, A. (2015). "MPM modelling of landslides in brittle and unsaturated soils." Ph.D. thesis, Univeritat Politecnica de Catalunya, Univeritat Politecnica de Catalunya.
Yerro, A., Alonso, E., and Pinyol, N. M. (2013). "The Material Point Method: A promising computational tool in Geotechnics." *Proceedings of the 18th International Conference on Soil Mechanics and Geotechnical Engineering*, Paris.
Yerro, A., Pinyol, N. M., and Alonso, E. E. (2016). "Internal Progressive Failure in Deep-Seated Landslides." *Rock Mechanics and Rock Engineering*, 49, 2317–2332.
Yerro, A., Soga, K., and Bray, J. (2018). "Runout evaluation of Oso landslide with the material point method." *Canadian Geotechnical Journal*, 14(December), 1–14.

Downloaded from ascelibrary.org by VPI & SU on 06/08/20. Copyright ASCE. For personal use only; all rights reserved.

© ASCE

Zabala, F. and Alonso, E. (2011). “Progressive failure of Aznalcóllar dam using the material point method.” *Géotechnique*, 61(9), 795–808.
Zambrano-Cruzatty, L. and Yerro, A. (2019). “Numerical Simulation of a Free Fall Penetrometer Deployment Using the Material Point Method.” *2nd International Conference on the Material Point Method for Modelling Soil-Water-Structure Interaction*, 250–256.

Downloaded from ascelibrary.org by VPI & SU on 06/08/20. Copyright ASCE. For personal use only; all rights reserved.

© ASCE